

Mechanics of surface crosslinked poly(dimethyl siloxane) microstructure used for microcontact transfer printing

Chao Bao,¹ Zhifan Wang,¹ Yu Liu,² Yanning Zhang,³ Heng-Yong Nie,⁴ Woon-Ming Lau,⁵ Jun Mei¹

¹Chengdu Green Energy and Green Manufacturing Technology R&D Center, Chengdu 610299, China

²Jiangsu Key Lab of Advanced Food Manufacturing Equipment and Technology, School of Mechanical Engineering, Jiangnan University, Wuxi 214112, China

³School of Energy Science and Engineering, University of Electronic Science and Technology of China, Chengdu 611731, China

⁴Surface Science Western, University of Western Ontario, 999 Collip Circle, London, Ontario N6G 0J3, Canada

⁵School of Mathematics and Physics, University of Science and Technology Beijing, Beijing 100083, China

Correspondence to: Y. Liu (E-mail: yu.liu@vip.163.com) and Y. Zhang (E-mail: yanningz@csrc.ac.cn)

ABSTRACT: In microcontact transfer printing, the mechanics of the microstructure on an elastomeric stamp are crucial for obtaining a printed image with high feature resolution and repeatability. In this article, we are dedicating research efforts to visit a methodology for surface crosslinking a poly(dimethyl siloxane) microstructure, implemented by a hyperthermal hydrogen-induced crosslinking technique. The significant enhancement of Young's modulus of elastomeric base after the surface crosslinking is confirmed by consequent *ab initio* calculation and numerical simulation. Experiments based on compression test and forced lateral scanning have been done for verifying the enhanced mechanic stability. This work provides a surface treatment way for fabricating a printing stamp with high robustness and transfer printing quality. © 2017 Wiley Periodicals, Inc. *J. Appl. Polym. Sci.* **2017**, *134*, 45166.

KEYWORDS: elastomeric mechanics; microcontact transfer printing; stability; surface crosslinking

Received 21 November 2016; accepted 26 March 2017

DOI: 10.1002/app.45166

INTRODUCTION

Printing is emerging as an important manufacturing technique for either digital or mask-based preparation of micro or nanostructures. A variety of printing techniques have ballooned in the past decade, including screen printing, offset printing, inkjet printing, and vapor deposition printing.^{1–4} For most of them, there is a resolution limit hampering their extensive uses. For example, for a commonly studied inkjet printing, it is in face with clogging of jet nozzle after long-term uses, with printing resolutions limited at above 20 μm . Recently, microcontact transfer printing,⁵ also called “soft lithography,” has been developed as a most important representative out of the group of different patterning techniques, which is capable of fabricating fine structure at nanoscale.⁶ Wherein, a stamp, replicated from an etched silicon plate carrying an image, is brought into direct contact with a substrate and transfers an ink image onto the substrate surface with high resolutions at both of normal and lateral orientations.

A stamp is usually made from an elastomeric polymer, particularly poly(dimethyl siloxane) (PDMS), which allows for well-posed conformal contact with the substrate surface in further

combination with advantageous attributes including nontoxicity, low curing temperature, and high stability under chemical erosion.⁶ However, at the transfer printing step, conformal contact may degrade lateral resolutions and causes printed image being deviated from the originally designed pattern. Delamarche *et al.*⁷ pointed out the stability issue as associated with molded PDMS micropillars during contact printing, such as lateral collapse and vertical sagging, and gave an empirical relationship on the ratio of the height (H) to the width (D) of the pillar structure, $0.5 < H/D < 5$, for preventing structure instability as shown in Figure 1(a). If the ratio of the height to the width of the pillar structure is significantly large, the stamp easily collapses due to the contact force during inking or transferring. On the other hand, if the ratio is too low, insufficient relief exists on the stamp surface to withstand the pressing force.

In the past, some efforts have been done for implementing enhanced stability of the stamp design. For example, Schmid and Michel⁸ conducted the formulation of siloxane polymers from vinyl and hydrosilane end-linked polymer and vinyl and hydrosilane copolymers for high-resolution and high-accuracy printing. However, this method may fail from cracking during pressing and releasing processes, or high thermal expansion

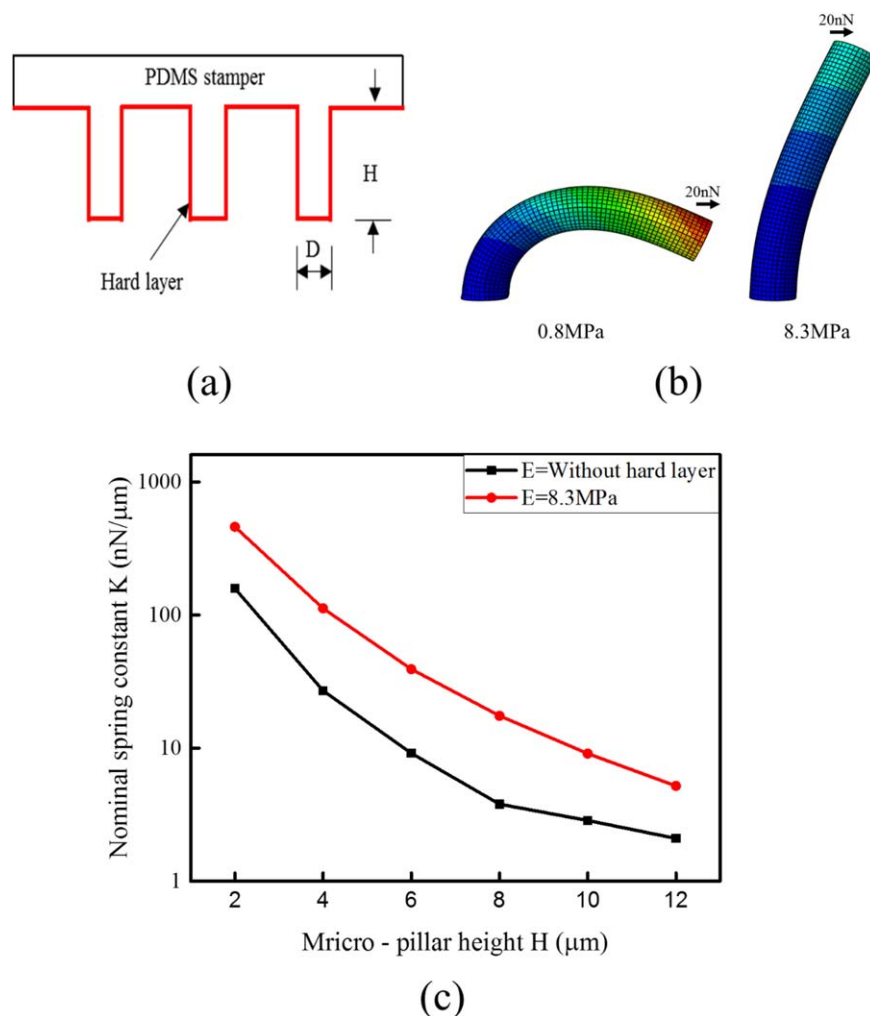


Figure 1. (a) Schematic of crosslinking micropillar structures on PDMS stamp with formation of a hard layer; (b) deformation of micropillar with and without surface crosslinking; and (c) stiffness (or stability) comparison of micropillar with and without surface crosslinking. [Color figure can be viewed at wileyonlinelibrary.com]

during curing, or nonuniform stamp distortions during conformal contact. Odom *et al.*⁹ built a strategy to fabricate a composite, two-layer stamp—a stiff layer (feature structure) supported by a flexible layer (roof structure) to extend the capability to print 50 to 100 nm features. For successful pattern transfer at nanoscale, Zhou *et al.*¹⁰ fabricated U-shaped stamp based on poly[(mercaptopropyl)methylsiloxane], which owns low thermal expansion with posed compliance in close and conformal contact with substrate surface¹¹. In consider of inks' compositions such as including organic solvents, the swelling of PDMS might be problematic for implementation of transfer printing with nanoscale resolution. And Teflon AF layer had to be introduced as a thin coating on the stamp surface to prevent the structure deforming.¹²

In this article, we are launching a hyperthermal hydrogen-induced crosslinking (HHIC)^{13–15} strategy for hardening the surface layer on the micropillars of PDMS stamp, as in Figure 1(a). Atomic force microscopy (AFM) method will be used to measure the mechanical properties for both bulk and micropillars. Then, *ab initio* calculations will be adopted for

understanding the effect of HHIC on the mechanic properties of PDMS at an atomic level. Finally, the effects of the HHIC enhancement for the micropillars will be measured by AFM-based method and compared by the simulation method.

EXPERIMENTAL

Throughout this work, a PDMS stamp with micropillar structure was first prepared by the replica method.⁵ To get a hydrophobic surface for easily peeling off PDMS stamps, the patterned silicon mold and control silicon wafer were silanized by tridecafluoro-1,1,2,2-tetrahydrooctyl-1-trichlorosilane. Patterned and control PDMS stamps without patterns were both experiencing a surface crosslinking treatment on a homebuilt HHIC system.¹⁶ The inside pressure of the HHIC reactor was pumped down to 6×10^{-4} Pa followed by filling with hydrogen gas at a velocity of 14 SCCM until the pressure was back up to 0.1 Pa. A negative electric field under the electron-cyclotron-resonance (ECR) microwave plasma chamber was used to accelerate the protons generated inside of ECR. The accelerated protons were collided with the hydrogen molecules

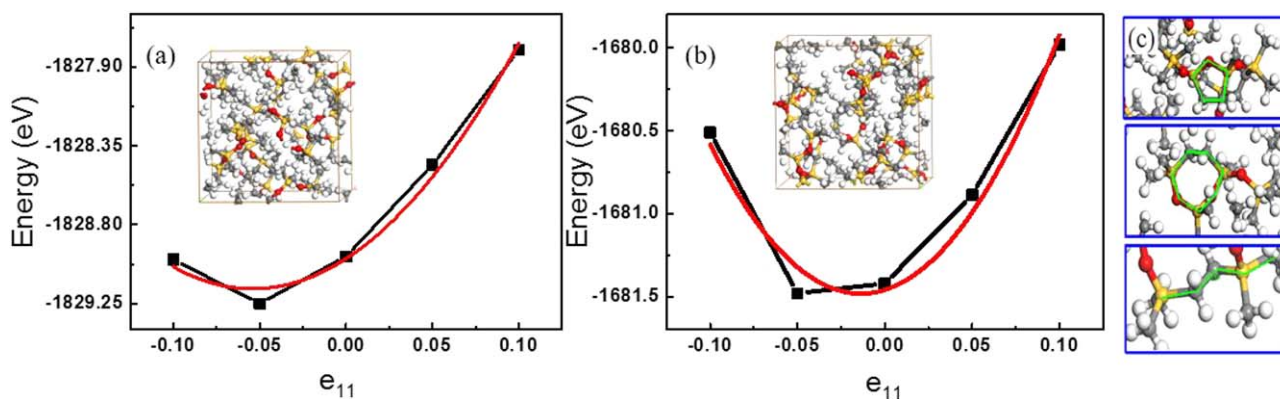


Figure 2. The elastic modulus of seven-chain systems (a) before and (b) after surface crosslinking. Insets show the configurations used for the elastic moduli calculations, where the grey, white, yellow, and red balls represent C, H, Si, and O atoms, respectively. Shown in (c) are examples of crosslinked PDMS local structures, as highlighted by the green lines. [Color figure can be viewed at wileyonlinelibrary.com]

in the drift zone that increased the energy of hydrogen molecules up to ~ 10 eV. Two inverse electric fields above the sample with a voltage of -50 V and $+100$ V, respectively were used to capture the residual electrons and protons. Finally, only neutral hydrogen projectiles can reach the sample to crosslink the molecules on the surface.

The mechanical stability of the HHIC treated PDMS stamp was simulated by the software Abaqus. Compression All *ab initio* calculations were carried out by using the Vienna Ab initio Simulation Package.¹⁷ The Perdew–Burke–Ernzerhof version of the generalized-gradient approximation¹⁸ was adopted to describe the exchange–correlation interaction among electrons, with the inclusion of the nonlocal van der Waals correction (vdW-DF).¹⁹ An energy cutoff of 500 eV was employed and only Γ -point was used to sample the Brillouin-zone.

The topography of pillar structure of the cross-sectioned PDMS stamp subjected to HHIC treatment and the control was studied with tapping mode of an AFM (MFP—Origin, Oxford Instrumentation Inc.), by randomly imaging a surface area of $20 \mu\text{m} \times 20 \mu\text{m}$ with a pixel density of 256×256 . Used in this experiment was a cantilever having a nominal spring constant of 2 N/m, a resonant frequency of 70 kHz and a tip radius of 9 nm. The different stamp samples were also imaged by SEM (S5200, Hitachi Inc.) as performed under a 5 kV acceleration voltage by a SEM) for studying their morphologies.

The mechanical stability of the cross-sectioned PDMS stamp subjected to HHIC treatment and the control was studied with contact mode and force mode of the AFM. Upon this study, morphology was first obtained with a scan rate of 1 Hz. And then, nine force curves were interpedently carried out on different locations of each samples through applying loading force up to 250 nN. Based on Hertz model,²⁰ the elastic modulus over the nine locations were calculated and analyzed statistically.

RESULTS AND DISCUSSION

To study the mechanical stability of the HHIC-treated PDMS stamp, the apparent elastic modulus E of PDMS after the HHIC

treatment was first measured based on the AFM force curve following the Hertz eq. (2):

$$F = \left(\frac{3}{4} E \sqrt{R} \right) \delta^{3/2} \quad (1)$$

where δ is the penetration depth of the AFM tip into the PDMS sample under indentation force F and R is the AFM tip radius, which was 9 nm used in this study (Asylum Research). And

$$\delta = z - \Delta z \quad (2)$$

where z is the cantilever displacement and Δz the deflection of the cantilever due to the compliance. From this AFM approach, the elastic moduli for control PDMS and the HHIC-treated PDMS were estimated to 0.8 and 8.3 MPa, respectively.

In *ab initio* calculations, seven PDMS chains with a molecular formula of $[\text{C}_2\text{H}_6\text{OSi}]_4$ for each chain were placed in a $16 \times 16 \times 16 \text{ \AA}^3$ box, keeping its density close to experimental value of 0.97 g/cm^3 .²¹ After structural optimization, the PDMS chains enwind with each other, as shown in the inset in Figure 2(a), but there is no any C—C bonds with a minimum C—C distance of 1.7 \AA . To imitate the crosslinked PDMS, four C—H bonds were randomly broken in each PDMS chain, so there are totally 28 methylenes in the supercell. After structural optimization, we found 14 C—C bonds formed between the methylene radicals within a bond length of 1.3 to 1.7 \AA , meaning that the seven PDMS chains were fully crosslinked, as shown in the inset in Figure 2(b). The average C—C bond is about 1.557 \AA , which is also consistent with experimental data.²² Interestingly, we see that C, Si, and O atoms form some ring, linear and crossed structures, as depicted in Figure 2(c), so as to link isolated PDMS chains to form a network.

Assuming that the seven-PDMS system is in a cubic symmetry, its elastic constant C_{11} can be obtained by $C_{11} = 2\Delta E/(V \times \delta^2)$,²³ where E is the total energy of the system, V is the equilibrium volume, and δ is its distortion along (001) direction. This method has been used for the determination of elastic constant of PVDF system.²⁴ We changed the lattice constant along (001) direction by a step of $\pm 5\%$ ($\delta = 0.05$) and made the atomic positions fully relaxed. The obtained energy change (ΔE) as a

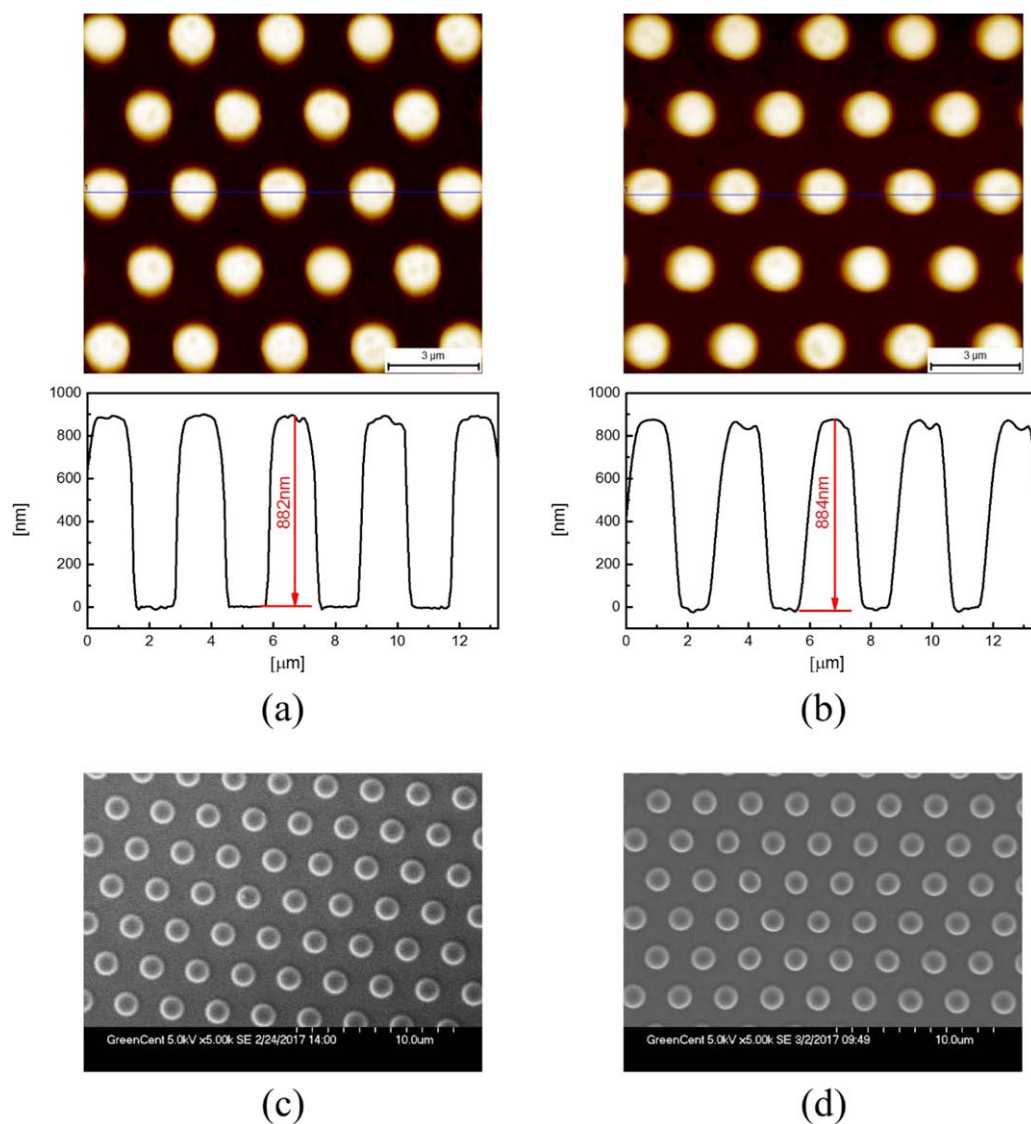


Figure 3. AFM height images of PDMS pillars for (a) control and (b) surface crosslinked stamps, respectively. And SEM morphology images of PDMS stamp for (c) control and (d) surface crosslinked, respectively. [Color figure can be viewed at wileyonlinelibrary.com]

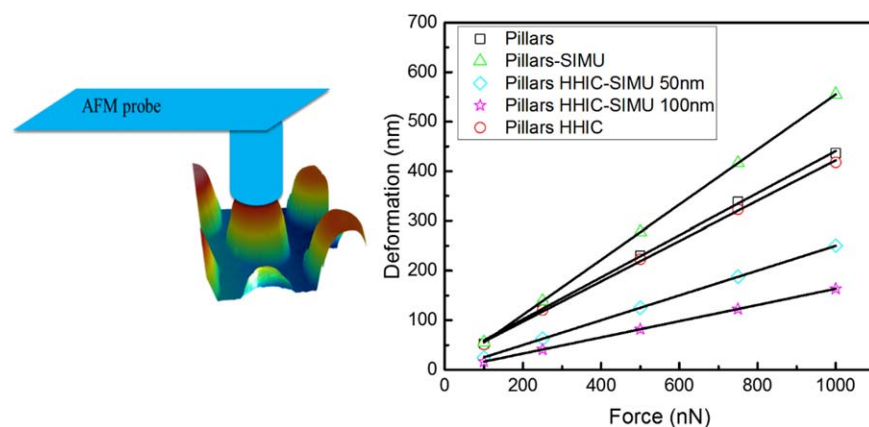


Figure 4. AFM-based method for measuring the deformation of control and surface crosslinked micropillars under different loading force. The triangle- and star-shape points represent the simulation results without and with a hard layer, respectively, while the square- and circle-shape points represent the AFM compress test results before and after HHIC treatment, respectively. [Color figure can be viewed at wileyonlinelibrary.com]

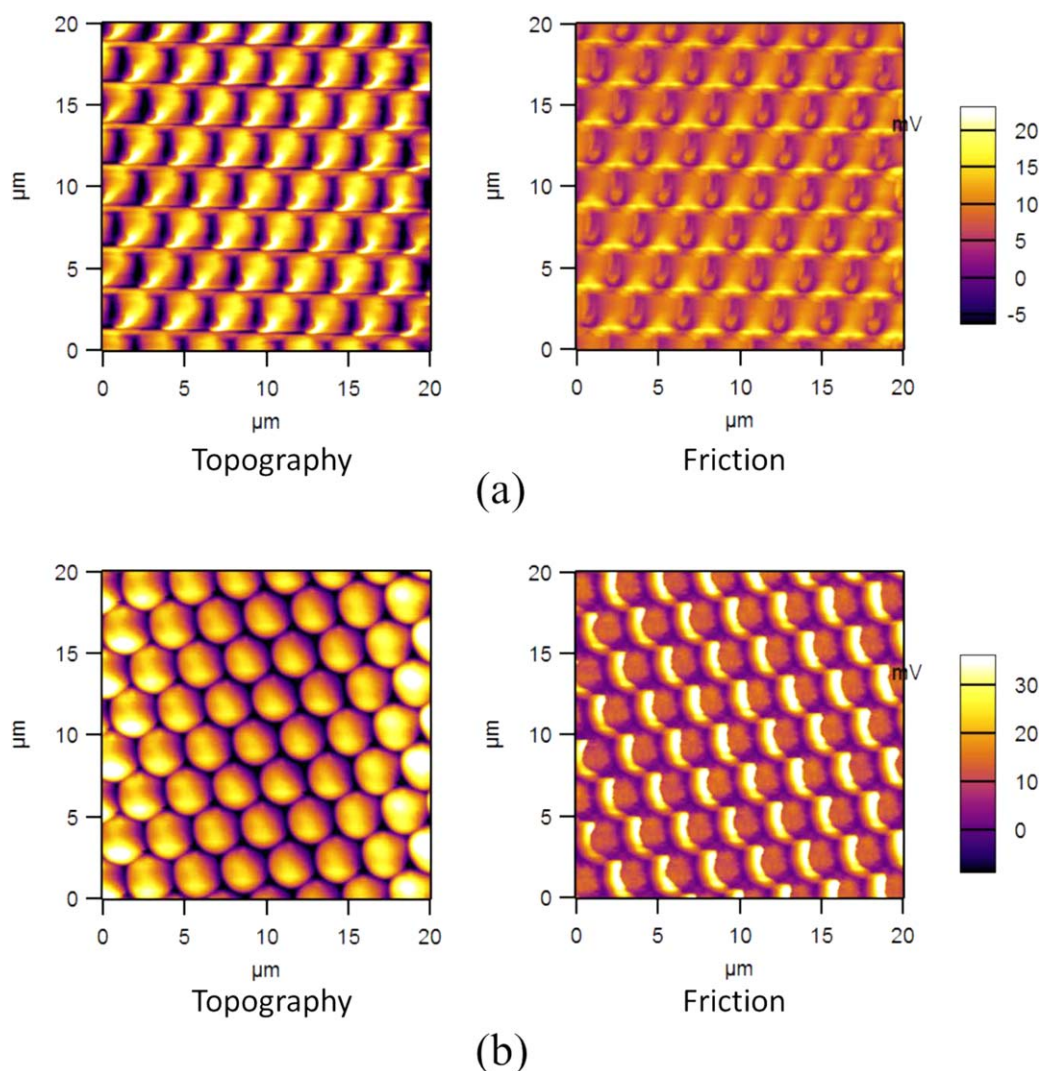


Figure 5. AFM-based method for measuring the morphological and friction images on control (a) and surface crosslinked (b) PDMS stamps under traction force of 75 nN. [Color figure can be viewed at wileyonlinelibrary.com]

dependence of δ are shown in Figure 2(a,b). The simulated results are trying to employ the theoretical method to demonstrate that the crosslink of PDMS caused by HHIC would increase the elastic modulus of PDMS. The calculated C_{11} are 9.07 GPa and 18.5 GPa for the system before and after HHIC treatment, respectively. As to the significant difference between the calculated and experimental results, it can be explained as: the elastic modulus calculated by *ab initio* method is based on an ideal periodic structure filled with pure PDMS short chains. The number of chains in the unit cell of the periodic structure is set as 7, which is limited by the calculation cost. In experiments, the used PDMS is typically blended with curing agent and the elastic modulus is based on the deformation of all the long chains, which cannot be effectively simulated by *ab initio* method due to the huge amount of computation cost. However, qualitatively we can see that, after 40% crosslinking, the elastic constant of PDMS increases by 100%.

When referring to a PDMS stamp design in Ref. 22, we modeled a pillar with a diameter $D=2\ \mu\text{m}$ and a height $H=12$

μm , i.e., $H/D=6$, and studied its stability with increasing H/D ratio under a surface traction force of 20 nN.^{25,26} As shown in the left panel in Figure 1(b), the pillar bends obviously under this surface traction force. Then we built a hard out-layer with a thickness of $\sim 0.1\ \mu\text{m}$ ¹¹ to mimic the enhanced surface stiffness of the pillar after HHIC treatment. We see from the middle and right panels in Figure 1(b) that even for $H/D=6$ which had clearly exceeded a critical point (the upper limit = 5) in the literature,⁵ we could still maintain an equivalent stability with nominal spring constant (the slope of the calculated force-displacement curve under traction force)²⁵ of $K \approx 16\ \text{nN}/\mu\text{m}$ on the HHIC treated pillar structure, as shown in Figure 1(b,c).

After the HHIC treatment on fabricated PDMS stamp, the micropillar was first imaged by tapping mode AFM, with the height of $\sim 884\ \text{nm}$, in close with that on the control PDMS stamp sample of $\sim 882\ \text{nm}$, as in Figure 3. Meanwhile, we applied SEM for imaging a larger surface area on the stamp surface and there was no any visible change on structural integrity after HHIC treatment. These results indicated that our

technique retained the major physical topography of the micropillar structures, which is important for preserving printing resolution from the design stage. In a further study toward mechanic stability of a single pillar, an AFM plateau tip PL2-FMR-10 (NANOSENSOR, Inc.) with nominal spring constant of 2 N/m was utilized and the deformation measurement results were shown in Figure 4. The flat front surface of the tip guaranteed the good compression test. Based on the morphological image, a micropillar was randomly selected and pressed under the AFM force mode with only experiencing an elastic deformation. The displacements of Z-sensor with an applied loading force from 100 to 1000 nN were recorded for calculating the deformations based on eq. (2). The deformation curve for the surface crosslinked elastomeric pillar showed smaller slope than that for the control sample and indicated the higher mechanic stability under loading force.

We further included Young's modulus, loading force and pillar dimension, as obtained from the experiments, into theoretical modeling for studying the impacts from different surface crosslinking depth on stability of a pillar, which has the width of 1.5 μm and height of 0.88 μm . First, as shown in Figure 4, there is a visible deviation between the deformation curve "Pillars - SIMU" for simulation and the one "Pillars" for experiment. It would be due to several reasons. The thermal calibration method on spring constant for the AFM cantilever did not really tell the exact value for the loading force as used in theoretical simulation. The method has its uncertainty up to 20%.²⁷ Secondly, geometric nonuniformity for a microfabricated pillar was not an ideally cylindrical shape and it suppressed measured slope for the deformation curve. In addition, measurement of the Young's modulus was obtained from a bulk PDMS film not directly from the pillar itself, as well as the indentation test had its own uncertainty.²⁸ From the simulation results, it is not surprising that the pillar with thinner surface-crosslinked layer had a worse stability. This could also help us understanding another possible reason for the disagreement between experimental and simulated curves that our surface crosslinking technique might not effectively treat the side walls of the pillar. There is a next step task for us to establish an angular HHIC on the stamp to secure treatment effectiveness on the side walls.

We further designed experiments, through carrying out friction imaging on HHIC treated sample and the control one, for characterizing the stability enhancement under traction force as simulated in Figure 1. In this study, same type of AFM plateau tip PL2-FMR-10 was utilized for establishing enough traction contact for deforming the pillar, when the tip is operating at lateral scanning mode with large contact loading force, such as up to 75 nN. During lateral contact scanning, each single pillar on the stamp experienced a large traction force and deformed accordingly. As a result, there is no success on obtaining a good topographic and friction images on the control PDMS stamp as shown in Figure 5(a) due to its low modulus or bad stability. In contrast, the HHIC treated PDMS stamp can be still clearly imaged without any deformation as in Figure 5(b). It provides another evidence on the enhanced stability of PDMS stamp after HHIC treatment.

CONCLUSIONS

In this work, surface crosslinking was introduced for hardening micropillars of PDMS stamp, through applying HHIC technique for selectively breaking C—H bonds and forming C—C bonds.¹⁸ *Ab initio* calculation was employed as an atomic level description of the surface crosslinking-induced modulus enhancement on the PDMS base. Thereafter, both of theoretical simulation and experimental tests were implemented for verifying the accessibility for our proposed surface crosslinking to prompt stability of micropillar structures.

ACKNOWLEDGMENTS

This work is sponsored by National Natural Science Foundation of China (Grant Nos. 51475484 and 61574131) and China Postdoctoral Science Foundation (Grants No. 2016M592703).

REFERENCES

1. Krebs, F. C. *Org. Electron. Phys. Mater. Appl.* **2009**, *10*, 761.
2. Nakata, K.; Fujishima, A. *J. Photochem. Photobiol. C Photochem. Rev.* **2012**, *13*, 169.
3. Sumerel, J. L.; Deravi, L. F.; Wright, D. W.; Dimatix, F.; Clara, S. *NSTI Nanotechnology* **2007**, *1*, 271.
4. Romanos, G. E.; Athanasekou, C. P.; Katsaros, F. K.; Kanellopoulos, N. K.; Dionysiou, D. D.; Likodimos, V.; Falaras, P. *J. Hazard. Mater.* **2012**, *211*, 304.
5. Qin, D.; Xia, Y.; Whitesides, G. M. *Nat. Protoc.* **2010**, *5*, 491.
6. Kumar, A.; Whitesides, G. M. *Appl. Phys. Lett.* **1993**, *63*, 2002.
7. Delamarque, E.; Schmid, H.; Michel, B.; Biebuyck, H. *Adv. Mater.* **1997**, *9*, 741.
8. Schmid, H.; Michel, B. *Macromolecules* **2000**, *33*, 3042.
9. Odom, T. W.; Love, J. C.; Wolfe, D. B.; Paul, K. E.; Whitesides, G. M. *Langmuir* **2002**, *18*, 5314.
10. Zhou, F.; Wang, C.; Dong, B.; Chen, X.; Zhang, Z.; Sun, C. *Opt. Express* **2016**, *24*, 6367.
11. Stuart, C.; Park, H. K.; Chen, Y. *Small* **2010**, *6*, 1663.
12. Choi, W. M.; Park, O. O. *Microelectron. Eng.* **2004**, *73*, 178.
13. Thompson, D. B.; Trebicky, T.; Crewdson, P.; McEachran, M. J.; Stojcevic, G.; Arsenaault, G.; Lau, W. M.; Gillies, E. R. *Langmuir* **2011**, *27*, 14820.
14. Bao, C.; Xu, K. Q.; Tang, C. Y.; Lau, W. M.; Yin, C.; Bin, Zhu, Y.; Mei, J.; Lee, J.; Hui, D.; Nie, H. Y.; Liu, Y. *ACS Appl. Mater. Interfaces* **2015**, *7*, 8515.
15. Liu, Y.; Yang, D. Q.; Nie, H.-Y.; Lau, W. M.; Yang, J. *J. Chem. Phys.* **2011**, *134*, 74704.
16. Man, C.; Jiang, P.; Wong, K.; Zhao, Y.; Tang, C.; Fan, M.; Lau, W.; Mei, J.; Li, S.; Liu, H.; Hui, D. *J. Mater. Chem. A* **2014**, *2*, 11980.
17. Kresse, G.; Furthmüller, J. *Comput. Mater. Sci.* **1996**, *6*, 15.
18. Perdew, J. P. J.; Burke, K.; Ernzerhof, M. *J. Phys. Rev. Lett.* **1996**, *77*, 3865.

19. Klime, J.; Bowler, D. R.; Michaelides, A. *Phys. Rev. B: Condens. Matter* **2011**, *83*, 195131.
20. Lin, L. Y.; Kim, D. E. *Polym. Test.* **2012**, *31*, 926.
21. Bates, O. K. *Ind. Eng. Chem.* **1949**, *41*, 1966.
22. Lide, D. R. *CRC Handbook of Chemistry and Physics: A Ready-Reference Book of Chemical and Physical Data: 1993-1994*. CRC press, **1993**.
23. Wang, S. Q.; Ye, H. Q. *J. Phys. Condens. Matter* **2003**, *15*, 5307.
24. Pei, Y.; Zeng, X. C. *J. Appl. Phys.* **2011**, *109*, 93514.
25. Yang, M. T.; Fu, J.; Wang, Y.; Desai, R. A.; Chen, C. S. *Nat. Protoc.* **2011**, *6*, 187.
26. Biebuyck, H.; Larsen, H. B.; Delamarche, E.; Michel, B. *IBM J. Res. Dev.* **1997**, *41*, 159.
27. Burnham, N. A.; Chen, X.; Hodges, C. S.; Matei, G. A.; Thoreson, E. J.; Roberts, C. J.; Davies, M. C.; Tandler, S. J. B. *Nanotechnology* **2003**, *14*, 1.
28. White, C. C.; Vanlandingham, M. R.; Drzal, P. L.; Chang, N. K.; Chang, S. H. *J. Polym. Sci. Part B: Polym. Phys.* **2005**, *43*, 1812.